

A Horizontal Vane Radiometer: Experiment, Theory, and Simulation

David Wolfe¹⁾, Andres Larraza^{1,a)}, and Alejandro Garcia²⁾

¹*Department of Physics, Naval Postgraduate School, Monterey CA 93940, USA*

²*Department of Physics and Astronomy, San Jose State University, San Jose CA 95152, USA*

The existence of two motive forces on a Crookes radiometer has complicated the investigation of either force independently. The thermal creep shear force in particular has been subject to differing interpretations of the direction in which it acts and its order of magnitude. In this article we provide a horizontal vane radiometer design which isolates the thermal creep shear force. The horizontal vane radiometer is explored through experiment, kinetic theory, and the Direct Simulation Monte Carlo (DSMC) method. The qualitative agreement between the three methods of investigation is good except for a dependence of the force on the width of the vane even when the temperature gradient is narrower than the vane which is present in the DSMC method results but not in the theory. The experimental results qualitatively resemble the theory. The quantitative agreement between the three methods of investigation is better than an order of magnitude in the cases examined. We find that the thermal creep force acts from the hot side to the cold side of the vane. We also find the peak in the radiometer's angular speed as a function of pressure is explained as much by the behavior of the drag force as by the behavior of the thermal creep force.

Keywords – Rarefied Gas Flows: Kinetic Theory, Numerical Methods

I. THE CROOKES RADIOMETER

Thermal transpiration or thermal creep is the flow of a gas over a surface due to a temperature gradient in the gas parallel to the surface. The force on the gas is equal and

^a Author to whom correspondence should be addressed. Electronic mail: larraza@nps.edu

opposite to the force on the surface. The force exerted on a surface by a gas with a temperature gradient is thus called the thermal creep force. The force is most famously demonstrated by the Crookes radiometer shown in figure 1.



Fig. 1. A Crookes Radiometer. One side of the vanes is white and the other is black. The chamber is partially evacuated. When exposed to bright light the black side of the vanes heats more quickly than the white side and the vanes rotate with the white side leading. Image by Jamian, 2012.

William Crookes published the atomic weight of Thallium in 1873. He weighed Thallium salts at atmospheric pressure and reduced pressure to quantify the buoyant force on his sample and determine what the weight would be in a perfect vacuum. He found that the weight measured at reduced pressures was sensitive to the light source he used to illuminate the scale. At the time it was believed that a hot object would weigh less than a cold object of similar mass because of upward air flow near the hot object or condensation on the cold object. [1] Crookes recognized these effects should decrease with decreasing pressure, but the effect he was observing did not. He designed the Crookes radiometer and other experiments to study the effect. In 1874 he ascribed the observed motion to repulsion by radiant heat which he theorized is present at all pressures but masked by air currents at higher pressures. [2] This is not the correct explanation of

the motion. Though radiation pressure does exist, it produces a small force and would tend to move the vanes with the black side leading contrary to the observed motion.

The same year Crookes published his results and analysis, Osbourne Reynolds published an analysis ascribing the effects to the transfer of momentum between the surface and gas molecules during evaporation, condensation, and heat transfer. An evaporating molecule leaves the surface with a certain momentum and the surface gains an equal and opposite momentum. A molecule undergoing condensation arrives with a certain momentum which is transferred to the surface. A molecule that transfers heat with a surface during a collision departs with a different momentum than with which it arrived the balance of which is conserved by transfer to or from the surface. [3]

Reynolds continued to study the transfer of momentum between a surface and a gas during heat transfer by experimenting with a porous plate with its two sides held at different temperatures. He was able to conduct his experiments at atmospheric pressure because the ratio of a characteristic length of the pores to the mean free path of air at atmospheric pressure is similar to the ratio of the characteristic length of a vane in a Crookes radiometer to the mean free path of air at the pressures where motion can be observed. He found that gas would flow through the pores from the cold side of the plate to the hot side of the plate and named this flow “thermal transpiration” in 1879. Molecules entering the pores from the cold side of the plate tend to gain heat and therefore velocity as they travel through the pore while molecules entering the pores from the hot side of the plate tend to lose heat and therefore velocity as they travel through the pore. These effects combine for a net velocity and flow from the cold side to the hot side. This same flow occurs over the edge of the vanes in a Crookes radiometer creating a thermal creep force on the vane directed from the hot side to the cold side. [4]

Also in 1879 but after reading Reynolds’ paper, James Maxwell further refined the theory of thermal transpiration by considering the details of the collisions between gas molecules and the surface. Maxwell considered two types of collisions. Reflected gases behave as if the surface was perfectly smooth and elastic. No energy is transferred between a reflected gas and the surface, and the tangential components of the molecules’ velocity are unchanged by the collision. Reflected gas does not contribute to thermal

transpiration. Absorbed-and-evaporated gases behave as if they were “entangled in the stratum of spheres” that Maxwell imagined coving the surface. Energy is transferred between an absorbed-and-evaporated gas and the surface. Absorbed-and-evaporated gas molecules leave the surface in a random direction with a speed equivalent to the surface temperature. Absorbed-and-evaporated gas is responsible for thermal transpiration. The magnitude of the thermal transpiration effect is thus related to the ratio of the number of gas molecules that are absorbed-and-evaporated to the total number of gas-surface collisions in a sample. [5] This ratio is called the accommodation coefficient. Other models use separate accommodation coefficients for energy, normal momentum, and tangential momentum calculations. The Maxwell model which we will use throughout this paper implies those values are the same.

Thermal creep is a shear force acting on the edges of the vanes in a Crookes radiometer. In 1924, Albert Einstein identified a normal force acting on the perimeter of the vertical faces as well. He imagined a chamber of rarified gas with a temperature gradient and no mass flow. A flat surface smaller than a mean free path of the gas placed in the chamber normal to the temperature gradient would experience a force towards the cold side as the same number of molecules per unit time would collide with it from the cold side as from the hot side because of the no mass flow requirement while the particles coming from the hot side would have a higher velocity. A flat surface larger than a mean free path of the gas in the same chamber oriented in the same way would not have a net force on its center once the pressure in the chamber had time to equalize and reestablished the no mass flow requirement. There would nevertheless be a transition region between the center of the object where no net force is experienced and the region beyond the surface where a small surface placed in the chamber would experience a force. This transition occurs over a mean free path wide perimeter of the surface. The vanes of the Crookes radiometer have a net normal force in this perimeter directed from the hot side to the cold side. [6]

Thermal creep and the Einstein effect provide the theoretical bases for the two motive forces on the Crookes radiometer. Subsequent work on the topic has focused on mathematical refinement of the theories and novel radiometer designs. A thorough review

of this work can be found in reference [7]. One novel design is the Hettner radiometer shown in figure 2. In 1924, M. Czerny and G. Hettner designed an experiment to measure the shear pressure or force on a plate with a uniform temperature from the thermal creep caused by a parallel plate with a temperature gradient. [8] This design does not experience the Einstein effect because the plate face is parallel to the temperature gradient.

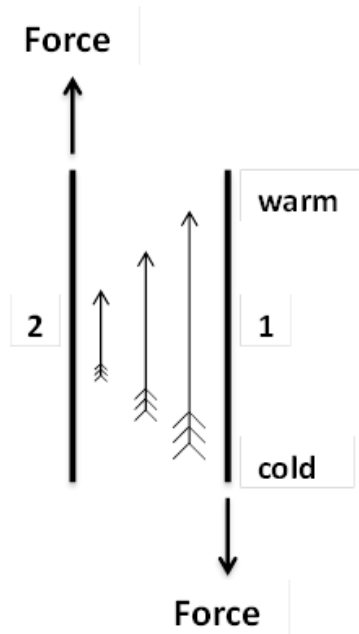


Fig. 2. Hettner Radiometer. Plate 1 has a temperature gradient and plate 2 has a uniform temperature. The temperature gradient establishes thermal transpiration (arrows with fletchings).

II. A HORIZONTAL VANE RADIOMETER EXPERIMENT

We designed a horizontal vane radiometer shown in figure 3 which like the Hettner radiometer has the temperature gradient parallel to the vane face but which like the Crookes radiometer is free to rotate around a spindle.

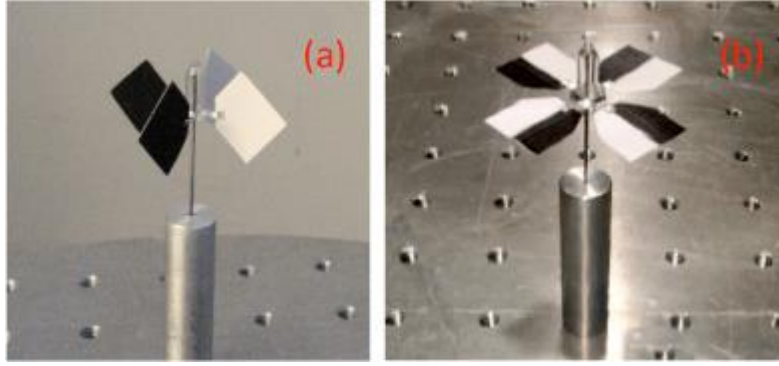


Fig. 3. The Crookes and Horizontal Vane Radiometers. (a) The Crookes radiometer experiences thermal creep forces and the Einstein effect. (b) The horizontal vane radiometer experiences thermal creep forces but no Einstein effect.

The angular speeds of horizontal vane radiometers were observed over a range of pressures with mean free paths from 5 mm to 0.2 mm. Two types of horizontal vane radiometers were constructed. The narrow vane radiometer had 8 mm by 16 mm vanes. The wide vane radiometer had 16 mm by 16 mm vanes. The vanes were constructed from high gloss photo paper. Half of the non-glossy side was printed with black LaserJet ink. Two pieces of paper cut into the shape of the vanes were glued together glossy side to glossy side so that both the upper and lower horizontal surfaces would have a white side and a black side. The vanes on both radiometers were connected to the spindle with 4 mm stems.

A high intensity radiant heat projector was used to illuminate the radiometers. The temperature profile that developed on the vanes when illuminated was observed with a FLIR SC8200 camera outside of the vacuum chamber and a FLIR ThermoVision A20 camera inside of the vacuum chamber. The temperature profile was not observed to be sensitive to pressure. Under illumination, the vanes developed a 9 K temperature difference between the black and the white side with the transition in temperature mostly occurring in a sharp gradient in the center of the vane with a characteristic length of 3.5 mm. The radiometers were tested in a 18 inch diameter 12 inch high Pyrex bell jar on a highly reflective test stand so that both the upper and lower horizontal surfaces would be illuminated. Figure 4 reports the results of these experiments at the pressures tested. [9] The link [10] shows video of horizontal vane radiometers rotating at 10 mTorr

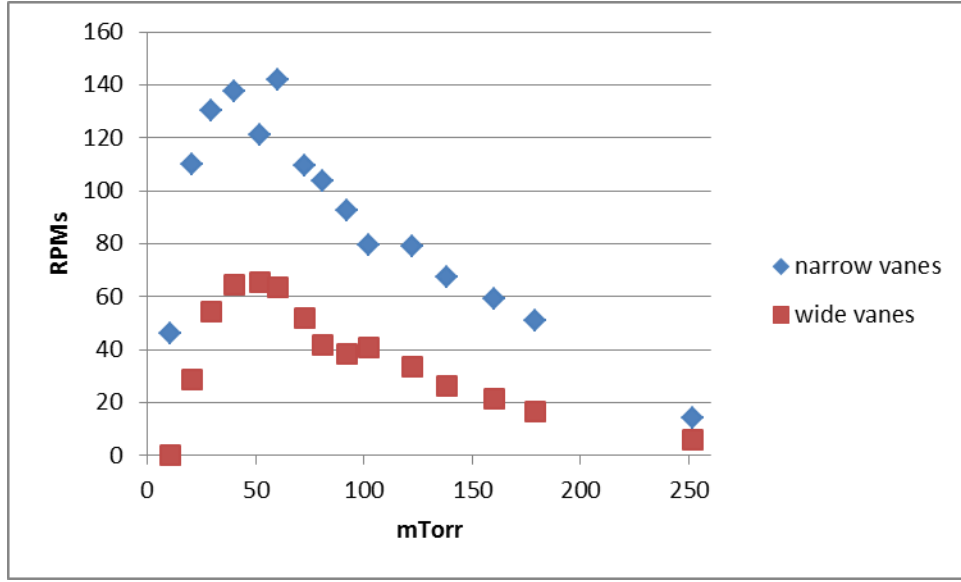


Fig 4. Angular Speed (experiment). The narrow vanes are 8mm by 16mm and the wide vanes are 16mm by 16mm. Both radiometers have four vanes. Vanes of both radiometers have a 4mm stem connecting them to the spindle axis. The temperature difference on the vanes is 9K. The characteristic length of the temperature gradient is 3.5mm. The observed motion is with the white (cold) side leading.

III. THE HORIZONTAL VANE RADIOMETER THEORY

The theory of thermal transpiration explains why the horizontal vane radiometer rotates, but an understanding of why the angular speed peaks and is a function of the vanes' widths requires careful examination of the details of both the thermal transpiration shear force and the drag force on the vanes.

A. THERMAL TRANSPIRATION

For an angular speed of 10 radians per second the furthest edges of the vanes will move a distance between 2 μm and 80 nm during a mean free time between collisions for the pressures in our experiment. Because these distances are small relative to the widths of the vanes in our experiment, a quasi-static approximation is justified for the calculation of the thermal creep force on a moving radiometer with the observed velocities.

Scandurra *et al.* derive an analytical formula for the thermal creep shear stress using the Chapman-Enskog method, [11]

$$\Delta p_{TC} = \frac{15}{64\sqrt{2}} \frac{k_B}{\sigma_{CS}} \frac{dT}{dy} \alpha, \quad (1)$$

where k_B is Boltzmann's constant, $\sigma_{CS} = \pi d^2$ is the hard-sphere collision cross section of the molecules with diameter d , dT/dy is the temperature gradient in the gas, and α is the accommodation coefficient.

The thermal creep force F_{TC} is this pressure multiplied by the area over which it acts A_{TC} . If L_{TC} is the length of a rectangle perpendicular to the temperature gradient and W_{TC} is the width along the temperature gradient, we have

$$F_{TC} = \Delta p_{TC} A_{TC} = \Delta p_{TC} L_{TC} W_{TC}. \quad (2)$$

Assuming the temperature gradient in the gas is roughly constant in the area where the thermal creep force acts, the temperature gradient term can be replaced by

$$\frac{dT}{dy} \approx \frac{\Delta T}{W_{Ggas}}, \quad (3)$$

where ΔT is the temperature difference between the hot and the cold sides of the surface and W_{Ggas} is the width of the temperature gradient in the gas.

The width of the temperature gradient established in a low-pressure gas by a surface with a temperature gradient is wider than the temperature gradient on the surface W_{Gsurf} by a length equal to the slip length, [12] or

$$W_{Ggas} = W_{Gsurf} + 2\lambda \frac{2-\alpha}{\alpha} \quad (4)$$

where λ is the mean free path of the gas and α is the accommodation coefficient. The mean free path is related to the particle number density n and collision cross section as $\lambda = 1/\sqrt{2}n\sigma_{CS}$.

The physical meaning of equation (4) can be understood by considering the two extreme values of α . When the accommodation equals zero, the width of the gradient in the gas is infinite. There is thus no gradient when there is no energy transfer between the surface and the gas. When the accommodation equals one, the width of the gradient in the gas is the width of the gradient on the surface plus two mean free paths. The gradient thus extends one mean free path further on each side in the gas than in the surface.

In the horizontal vane radiometer experiment, there are four temperature gradients in the plane of each vane shown in figure 5.

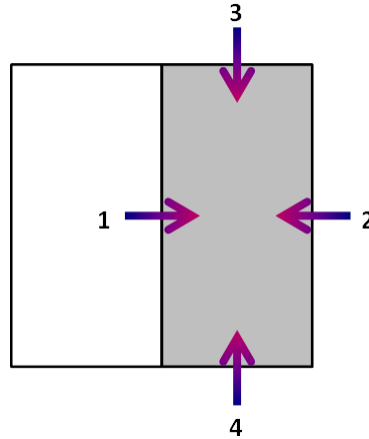


Fig 5. Temperature Gradients on a Horizontal Vane. The white (cold) side of the vane is assumed to have a temperature similar to ambient temperature and the grey (hot) side is warmer than ambient temperature.

Temperature gradient #1 causes the force F_{TC1} which causes the rotation of the radiometer and is a convenient starting point for the calculation of the total thermal creep force on the vane. We will treat the effects of the other temperature gradients as apparent modifications of the force from temperature gradient #1.

Temperature gradient #2 creates a force which opposes the rotation. The magnitude of this force is less than the magnitude of the force created by temperature gradient #1 because the portion of temperature gradient #2 which is not over the vane does not create a force, i.e.

$$F_{TC} = xF_{TC1}, \quad (5)$$

where x is a numerical factor between zero and one representing the fraction of the force from temperature gradient #1 which is offset by the force from temperature gradient #2.

The net force created by temperature gradients #3 and #4 is zero, but these gradients decrease the magnitude of temperature gradient #1 near the edges. This has the effect of decreasing the apparent length over which the net thermal creep pressure from temperature gradient #1 acts. The length correction is the slip length times the numerical factor β or

$$L_{TC}' = L_{TC1} - \beta\lambda \frac{2-\alpha}{\alpha}. \quad (6)$$

The width over which temperature gradient #1 acts is the smaller of either the width of the vane W_V or the width of the temperature gradient in the gas. Putting this together with equations (1) to (6) gives the following expression for the net thermal creep force on the two sides of a single vane in the horizontal vane radiometer experiment:

$$F_{TC} = \frac{x15}{32\sqrt{2}} \frac{k_B}{\sigma_{CS}} \Delta T \alpha L' \min\left(\frac{W_V}{W_{Gas}}, 1\right), \quad (7)$$

where L' is the length of the vane with the slip length correction and the force acts on both sides of the vane.

Figure 6 shows the net thermal creep force predicted by this equation for the vanes in the horizontal vane radiometer experiment assuming numerical factors of $x = 0.5$ and $\beta = 0.5$ for equations (5) and (6) and an accommodation coefficient of $\alpha = 0.6$. The accommodation value is the maximum value of the modified Boule formula for estimating clean surface accommodation coefficients. [13] We used the modified Boule formula because of the inability to find a tabulated value for the accommodation coefficient of paper in air. We chose the maximum value because the vanes were not “clean” and because the tabulated values that do exist for other materials often exceed the modified Boule formula estimate. An even higher value of the accommodation would result in the force rising more quickly as a function of pressure and asymptotically approaching a higher value. The pressure dependence of the force is a result of the slip length corrections in the width of the gradient in the gas and the apparent length of the vane.

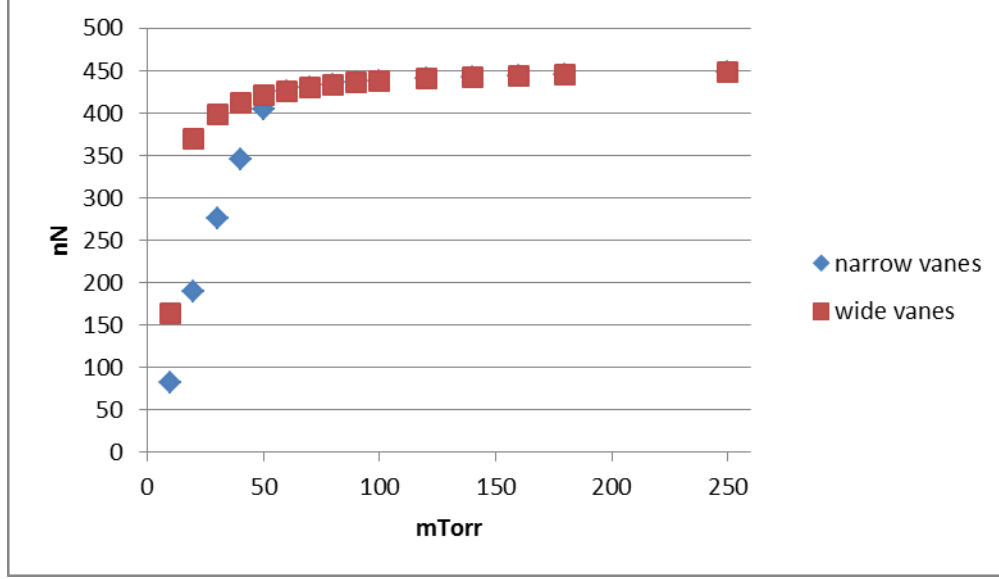


Fig 6. Thermal Creep Force (theory). The narrow vanes are 8mm by 16mm and the wide vanes are 16mm by 16mm. The temperature difference on both vanes is 9K. The characteristic length of the temperature gradient on the surface is 3.5mm. The accommodation coefficient is 0.6. At 60 mTorr and greater pressure the forces are similar on the narrow and wide vanes. A positive force is directed from the hot side to the cold side.

B. DRAG FORCE

The dominant drag force on a thin plate oriented parallel to the flow is skin friction. The Reynolds numbers for every trial in the horizontal vane radiometer experiment was less than 0.02. Therefore, for all the trials in this experiment the flow can be regarded as being in the Stokes' regime. The drag coefficient for Stokes' drag is proportional to the inverse of the Reynolds number.

$$C_D = \frac{\delta\mu}{\rho UW}, \quad (8)$$

where δ is a numerical factor, μ is the viscosity of the fluid, U is the characteristic flow velocity, W is the length over which the flow velocity varies (the width of the vane in this case), and ρ is the density of the fluid.

For thin plates oriented parallel to the flow, a theoretical value of 4.12 for δ has been calculated. [14] On the other hand, an experimental value of 5.91 has been observed. [15] Thus for uniform flow past a flat plate the Stokes drag force on both sides of the plate is

$$F_D = 2 \frac{1}{2} \rho U^2 C_D L W = 5.91 U \mu L, \quad (9)$$

where L is the dimension perpendicular to the flow (the length of the vane in this case).

The Stokes' drag equation does not take edge effects into account. Each edge parallel to the flow that is immersed in the fluid adds the empirically determined correction to the drag force equation [16]

$$F_{edge} = 1.6 U \mu W. \quad (10)$$

At low pressure there is an apparent decrease in the dynamic viscosity due to the slip length [12]

$$\mu' = \frac{\mu W}{W + 2\lambda \frac{2-\alpha}{\alpha}}. \quad (11)$$

Chapman's expression for the dynamic viscosity, [17]

$$\mu = \frac{5\pi}{32} \rho C \lambda, \quad (12)$$

which accounts for variable collision rate, improves on Maxwell's classical estimate, $\mu = \rho C \lambda / 3$. Here C is the mean speed of a gas molecule. Note that μ is pressure

independent. The substitutions $\rho = nm$ and $C = \sqrt{8k_B T / \pi m}$, where m is the molecular mass, express μ' in terms of kinetic theory quantities

$$\mu' = \frac{5\sqrt{\pi}}{16} \frac{\sqrt{mk_B TW}}{\sigma_{cs}W + \frac{\sqrt{2}}{n} \frac{2-\alpha}{\alpha}}. \quad (13)$$

It is not obvious that the slip length correction should apply to the drag on the edges but such correction is necessary for the edge correction to the drag force to be equal zero at zero pressure. We will assume the correction takes a similar form for both the skin friction and the edge drag.

For a uniformly rotating vane, including edge effects, the drag force is

$$F_D = \omega \left(L_s + \frac{L}{2} \right) \mu' (5.91L + 3.2W), \quad (14)$$

where L_s is the length of the stem. Figure 7 shows the drag force predicted by this equation for the vanes in the horizontal vane radiometer experiment at 10 rad/s.

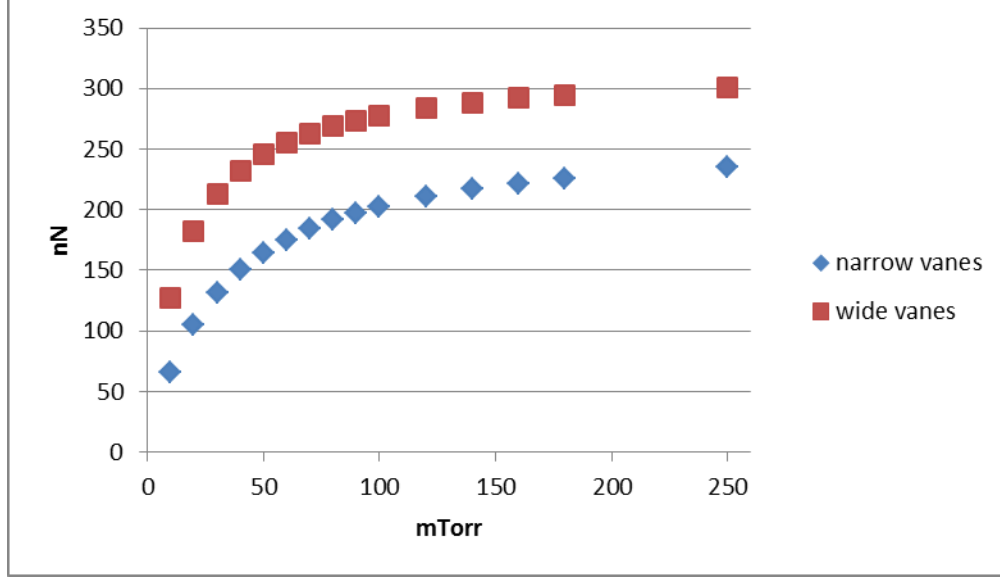


Fig 7. Drag Force at 10 rad/s (theory). The narrow vanes are 8mm by 16mm and the wide vanes are 16mm by 16mm. Both vanes have a 4mm stem connecting them to the spindle axis. The accommodation coefficient is 0.6.

C. ANGULAR SPEED

Assuming negligible mechanical friction in the spindle, the equilibrium angular speed ω of the horizontal vane radiometer occurs when the drag force F_D equals the thermal creep force F_{TC} . Because the drag force is linearly related to the angular speed, we can define the drag force per unit angular velocity f_D as

$$f_D = \frac{F_D}{\omega}. \quad (15)$$

Thus, in terms of thermal creep,

$$\omega = \frac{F_{TC}}{f_D}. \quad (16)$$

Since both forces will scale linearly with the number of vanes it is possible to examine the forces on a single vane to predict the angular speed of a radiometer with four vanes.

Figure 8 is the predicted angular velocity that results by using the expressions (14) and (7) in the above equation.

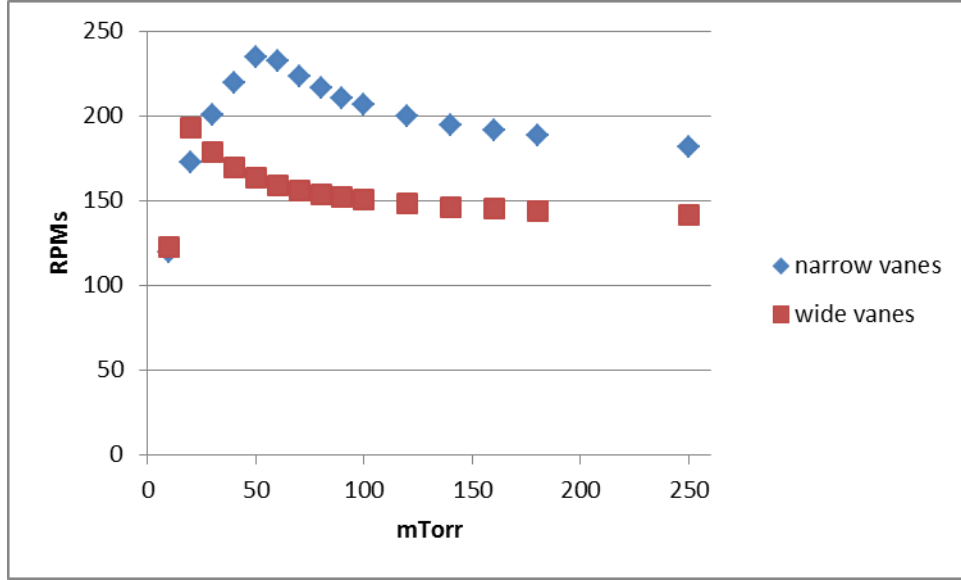


Fig 8. Angular Speed (theory). The narrow vanes are 8mm by 16mm and the wide vanes are 16mm by 16mm. Both vanes have a 4mm stem connecting them to the spindle axis. The temperature difference on both vanes is 9K. The characteristic length of the temperature gradient on the surface is 3.5mm. The accommodation coefficient is 0.6. Positive angular speed represents rotation with the cold side leading.

IV. HORIZONTAL VANE RADIOMETER SIMULATIONS

Direct Simulation Monte Carlo (DSMC) is a method of determining continuum properties of a fluid by simulating individual particles of the fluid. Simulation particles are weighted to represent multiple fluid particles to reduce computational effort. The Navier-Stokes equations of continuum gas dynamics are a computationally easier method of determining the same quantities but provide inaccurate results when the mean free path of the gas is greater than one-tenth of a representative length scale of the system (Knudsen number greater than 0.1). For this reason the DSMC method is most usefully applied to rarefied gases where the mean free path of the gas is of the same order or larger than a characteristic length of the system. [18]

DSMC programs divide the simulation space into grid cells. Particles are initially created in random locations with a Gaussian velocity distribution centered on an assigned fluid velocity. At each time step, particles move a distance equal to their velocity times the time step. The behavior of particles that reach the boundary of the simulation space is determined by the boundary conditions of the simulation. Particles that impact a surface in the simulation space undergo either specular or diffuse reflection depending on the simulation inputs. Momentum transfer between the surface and colliding particles is recorded for subsequent calculation of the pressure on the surface with the mass of a particle equaling the mass of a molecule times the number of molecules represented by a particle in the simulation.

After the particles have completed their motion, particles are randomly selected for collision. The probability that an individual particle will be selected for collision is determined by the mean free time between collisions of molecules in the gas being simulated divided by the time step. Collision partners are then chosen from within the same grid cell. The collision partners are assigned new velocities that conserve energy and momentum.

Statistical fluctuations in DSMC results can be averaged out by decreasing the number of molecules represented per simulation particle, increasing the amount of time simulated, or averaging the results of multiple trials. Systemic errors can be introduced by large grid sizes or time steps. The truncation error introduced by the grid size is proportional to the ratio squared of the length of a side of the grid cell to the mean free path of the gas. [19] The truncation error introduced by the time step is proportional to the ratio squared of the time step to the mean free time between collisions of molecules in the gas. [20]

SPARTA (Stochastic PARallel Rarefied-gas Time-accurate Analyzer) is an open-source DSMC program developed at Sandia National Laboratories. [21] [22] We used it in this research to determine separately the shear pressures caused by drag and thermal creep on vanes similar to those in the horizontal vane radiometer experiment at the range of pressures tested in the experiment. We used the February 21, 2015 version of SPARTA with one modification. The modification was the removal of the command to

terminate the trial if a particle collides with an interior surface of the vane. This feature was in the code to ensure objects in the simulation space are airtight, but occasionally the algorithm used by SPARTA to distinguish between interior and exterior collisions mistakenly classifies a collision in our geometry. We checked the simulated vanes for airtightness before running the trials on the modified program. We ran the trials on the Hamming supercomputer at the Naval Postgraduate School and the Spirit supercomputer at the Air Force Research Laboratory. Each trial took five thousand to 50 thousand CPU hours to complete.

A. THERMAL CREEP SIMULATIONS

We ran a total of 30 thermal creep simulations encompassing both the narrow vane and the wide vane at the 15 pressures tested in the experiment. In each trial, we simulated a single stationary vane and the shear pressure on the vane was the output. We divided each trial into 10 time segments which reported 10 separate average shear pressures. This confirmed the behavior was not transitory and allowed us to calculate a standard deviation between the 10 segments to quantify the uncertainty in the output.

In SPARTA, geometry objects have a single assigned temperature and cannot touch other objects. To simulate a vane with a temperature gradient, we created nine objects in the simulation space. Figure 9 is an overhead view of the wide and narrow vane as modeled in SPARTA.

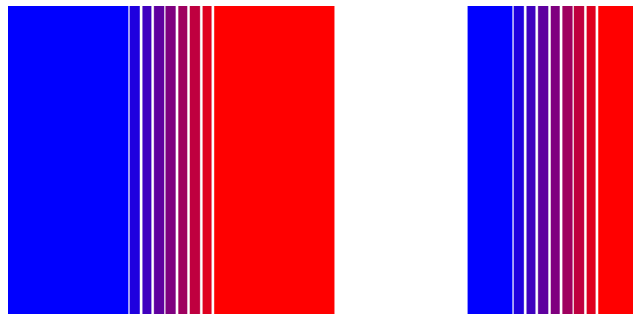


Fig. 9. Vanes as Modeled in SPARTA. The wide and narrow vanes are each divided into nine segments separated by two Angstroms. Each segment has a single assigned temperature.

The cold side of the vanes was assigned a temperature of 293 K. The hot side of the vanes was assigned a temperature of 302 K. Each intermediate segment was 1.125 K warmer than its colder neighbor. All nine rectangular boxes which comprised a vane were 16 mm long and 0.1 mm thick. The seven boxes in the gradient region were 0.5 mm wide which from equation (4) is thin enough to create a smooth gradient in the gas at all pressures simulated. The two end boxes were 6.25 mm wide for the wide vane and 2.25 mm wide for the narrow vane.

The simulation space was 18 mm by 26 mm by 10 mm for the narrow vane simulations and 26 mm by 26 mm by 10 mm for the wide vane simulations. This ensured at least one mean free path between the vane and the boundary at all pressures simulated. The boundary condition was inflow and outflow so particles whose trajectory took them outside the simulation space would no longer be simulated and new particles would be created and entered into the simulation space throughout the trial. The size of the grid cells was varied with pressure so that each edge of a grid cell equaled half of a mean free path in length. The total number of grid cells ranged from 280 for the narrow vane at 10 mTorr to over 6 million for the wide vane at 250 mTorr.

Particles were created with an initial average temperature of 293 K. 850 million particles were initially created in the narrow vane simulations and 1.2 billion particles were initially created in the wide vane simulations. This ensured there was an average of 200 particles per grid cell at the highest pressure trials. The lower pressure trials had more than 200 particles per grid cell since the grid cells were larger and fewer in the lower pressure trials. The number of molecules represented by a single simulation particle varied with pressure. This value varied from 1.8 million molecules per simulation particle at 10 mTorr to 45 million molecules per simulation particle at 250 mTorr. 79% of the particles were diatomic Nitrogen and 21% of the particles were diatomic Oxygen. We used the variable soft sphere collision model.

The time step was 100 ns. This value is one fourth the mean free time between collisions at 250 mTorr and a smaller fraction of the mean free time between collisions at lower pressures. Each simulation ran 100 thousand time steps. We calculated the force by

multiplying the shear pressure output by the area of the surfaces. Figure 10 shows the results of this calculation.

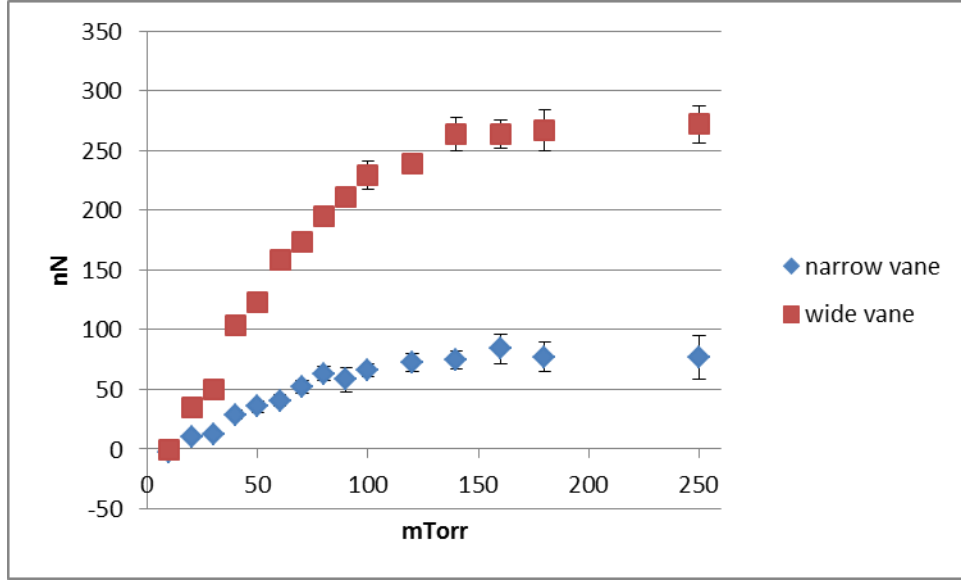


Fig 10. Thermal Creep Force (simulation). The narrow vane is 8mm by 16mm and the wide vane is 16mm by 16mm. The temperature difference on both vanes is 9K. The characteristic length of the temperature gradient on the surface is 3.5mm. The accommodation coefficient is 0.6. The range bars are the length of the standard deviation of the 10 segments of the trial at the reported pressure. Range bars that are not visible are hidden behind the identifying symbol. A positive force is directed from the hot side to the cold side. We believe the results at 10 mTorr to be spurious.

It is interesting to note that the values are negative at 10 mTorr (negative meaning pointing towards the hot side so that the radiometer would rotate with the black side leading). For the wide vane, the magnitude of the force is less than the standard deviation. For the narrow vane though, the force is -2.57 nN with a 1.63 nN standard deviation. None of the 10 time segments of the trial reported a positive force. This result is contrary to the experiment and theory, but similar results have been found by other researchers using the DSMC method to find thermal creep forces. [23] [24] To test the validity of this result we reran the simulation at 10 mTorr with the narrow vane in the larger simulation space used previously for the wide vane. The reported force was 2.31 nN in the positive direction (pointing toward the cold side). This demonstrates the result is sensitive to the size of the simulation space at 10 mTorr where there was a single mean free path between

the vane and the boundary of the simulation space and the negative results in our trials are not to be trusted. We reran the simulation in the same manner at 50 mTorr where there were five mean free paths between the vane and the boundary of the simulation space. The reported force was 36.61 nN in the positive direction which compares favorably with the previously determined force of 35.55 nN in the positive direction with a 9.64 nN standard deviation. This suggests the results are stable with respect to the size of the simulation space when there are multiple mean free paths between the vane and the boundary of the simulation space. The trials reported here at 20 mTorr and above include more than one mean free path between the vane and the boundary of the simulation space.

We also ran trials at selected pressures with a higher accommodation coefficient. A higher accommodation coefficient resulted in larger force values as expected. Figure 11 shows these results.

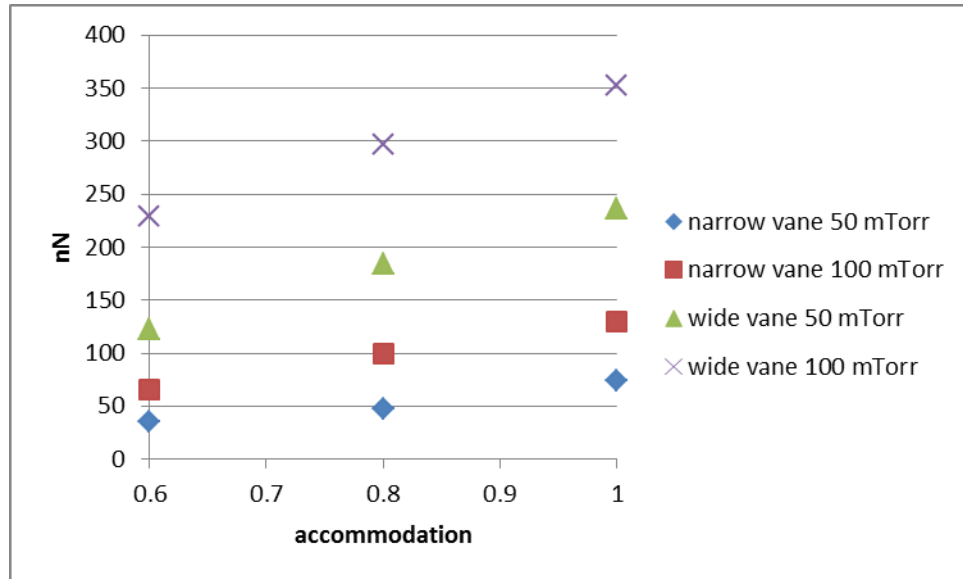


Fig. 11. Thermal Creep Force with varied accommodation (simulation). The narrow vanes are 8mm by 16mm and the wide vanes are 16mm by 16mm. The temperature difference on both vanes is 9K. The characteristic length of the temperature gradient on the surface is 3.5mm.

B. DRAG FORCE SIMULATIONS

We ran drag force simulations identical to the thermal creep simulations with two exceptions. Firstly, we modeled the vanes as a single rectangular object with a temperature of 293 K. Secondly, collisions between the vane and particles were calculated as if the vane were rotating at 10 radians per second around an axis 4 mm from the edge of the vane though the vane was not actually rotating in the simulation space. Figures 12 and 13 show the results of these trials.

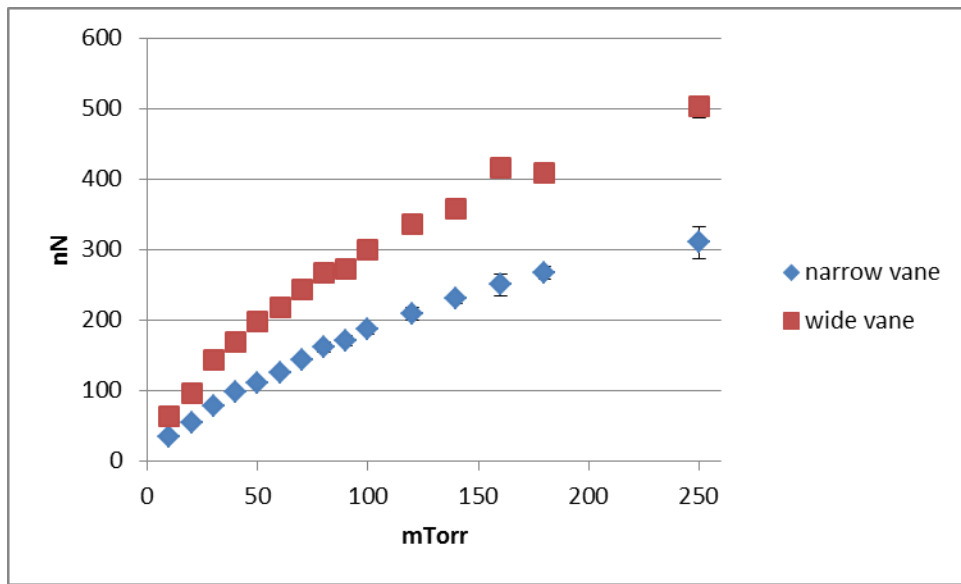


Fig 12. Drag Force at 10 rad/s (simulation). The narrow vane is 8mm by 16mm and the wide vane is 16mm by 16mm. Particle-surface collisions are calculated as if the vane is rotating about a point 4mm beyond its edge. The accommodation coefficient is 0.6.

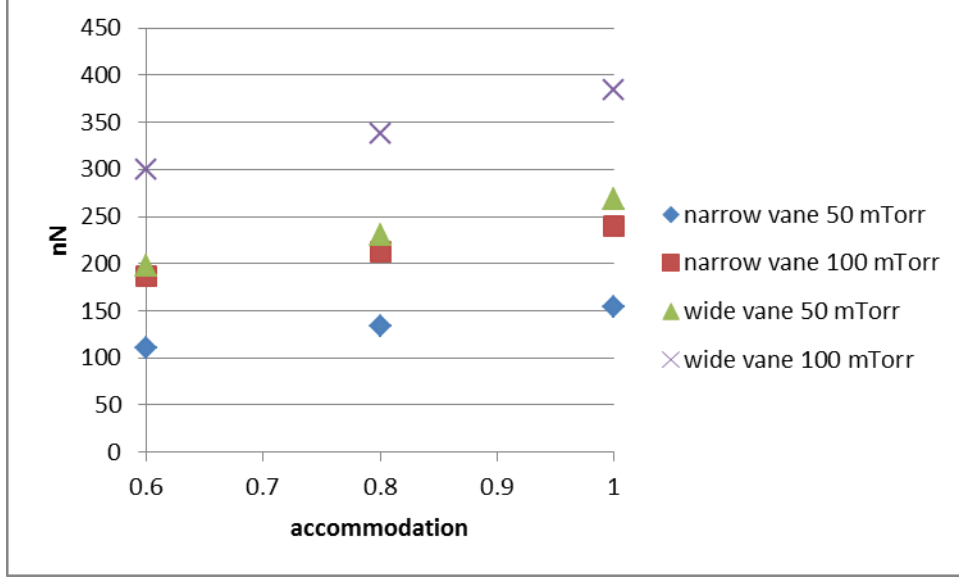


Fig 13. Drag Force with varied accommodation (simulation). The narrow vane is 8mm by 16mm and the wide vane is 16mm by 16mm. Particle-surface collisions are calculated as if the vane is rotating at 10 rad/s about a point 4mm beyond its edge.

C. ANGULAR SPEED

We calculated the angular speed predicted by the simulations in the same manner as we calculated the angular speed predicted by theory,

$$\omega = \omega_0 \frac{F_{TC}}{F_D}, \quad (17)$$

where ω_0 is the angular speed in the simulation. This method is possible because the drag force is linearly proportional to velocity at these pressures as seen in equation (14) and both forces scale linearly with the number of vanes on the radiometer. Figures 14 and 15 report the angular speed predicted by the simulations. We omitted the results at 10 mTorr because of the questionable nature of the results of our thermal creep simulations at that pressure.

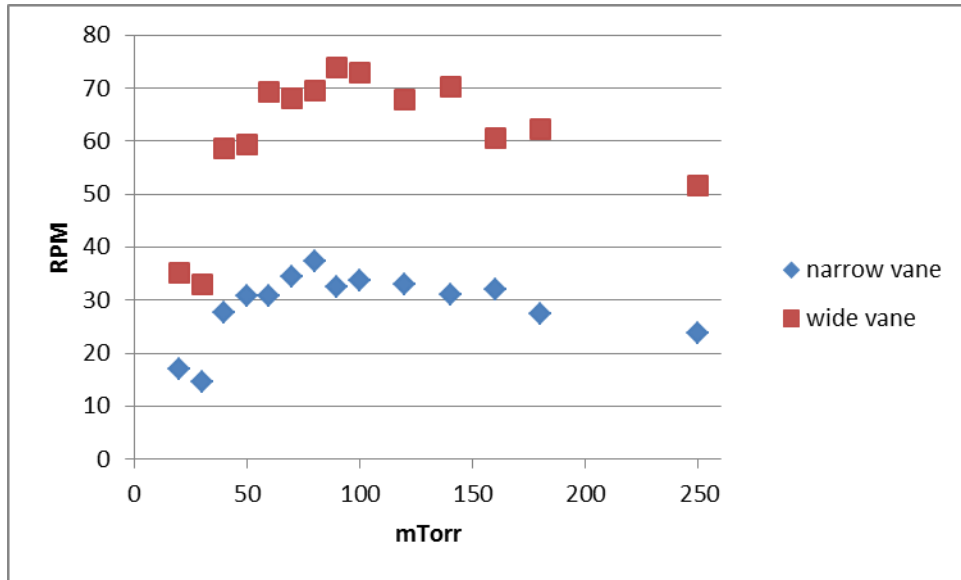


Fig 14. Angular Speed (simulation). The narrow vane is 8mm by 16mm and the wide vane is 16mm by 16mm. Both vanes have a 4mm stem connecting them to the spindle axis. The temperature difference on both vanes is 9K. The characteristic length of the temperature gradient on the surface is 3.5mm. The accommodation coefficient is 0.6. Positive angular speed represents rotation with the cold side leading.

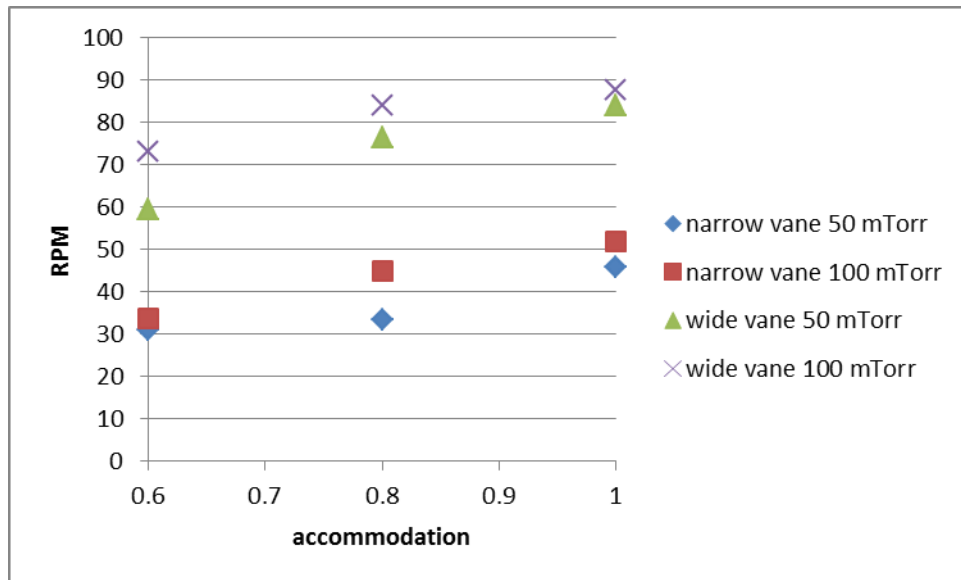


Fig. 15. Angular Speed with varied accommodation (simulation). The narrow vane is 8mm by 16mm and the wide vane is 16mm by 16mm. Both vanes have a 4mm stem connecting them to the spindle axis. The temperature difference on both vanes is 9K. The characteristic length of the temperature gradient on the surface is 3.5mm. Positive angular speed represents rotation with the cold side leading.

V. COMPARISON OF EXPERIMENT, THEORY, AND SIMULATIONS

In both the simulations and theory of the thermal creep force the force rises as a function of pressure at very low pressures then becomes almost constant as a function of pressure at relatively higher pressures. Quantitatively the differences at most pressures are less than an order of magnitude. A qualitative difference does stand out though. The simulations show the force on the narrow vane and the wide vane asymptotically approaching different values as the pressure increases while the theory has the force on the vanes asymptotically approaching similar values. Figures 16 and 17 compare the simulation results and theory predictions at the range of pressures examined. We omitted the simulation data points at 10 mTorr because of the questionable validity of our simulation parameters at that pressure.

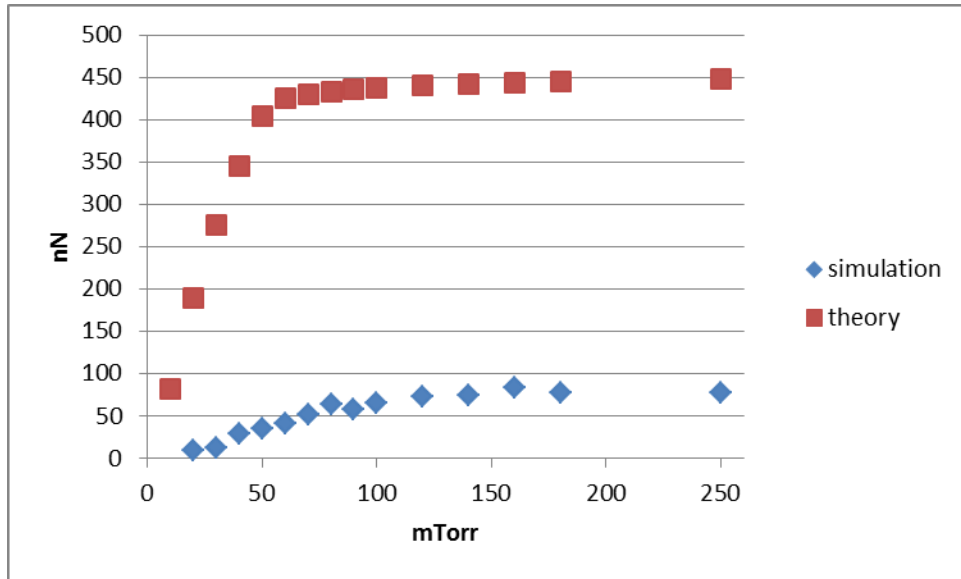


Fig 16. Narrow Vane Thermal Creep Force (simulation and theory). The vanes are 8mm by 16mm. The temperature difference on the vanes is 9K. The characteristic length of the temperature gradient on the surface is 3.5mm. The accommodation coefficient is 0.6. Positive force is directed from the hot side to the cold side.

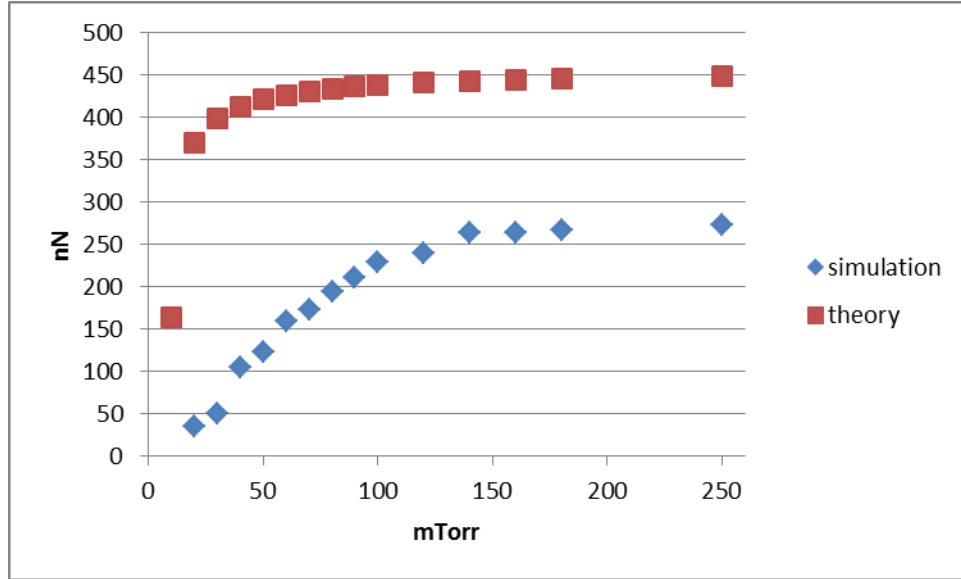


Fig. 17. Wide Vane Thermal Creep Force (simulation and theory). The vanes are 16mm by 16mm. The characteristic length of the temperature gradient on the surface is 3.5mm. The temperature difference on the vanes is 9K and the accommodation coefficient is 0.6. Positive force is directed from the hot side to the cold side.

In both the simulations and the theory of the drag force the force raises with pressure but the rate of increase decreases with pressure. The change in the rate of increase is more pronounced in the theory than the simulations. Quantitatively the agreement is very good around 100 mTorr and the differences are less than a factor of two at all pressures examined. Figures 18 and 19 compare the simulation results and theory predictions at the range of pressures examined.

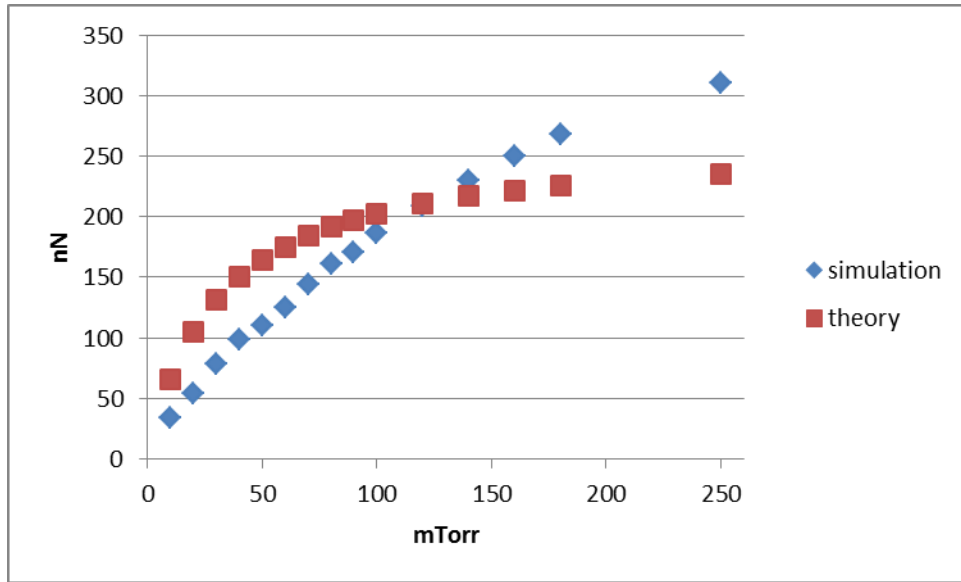


Fig. 18. Narrow Vane Drag Force (simulation and theory). The vanes are 8mm by 16mm and have a 4mm stem connecting them to the spindle axis. They are rotating at 10 rad/s. The accommodation coefficient is 0.6.

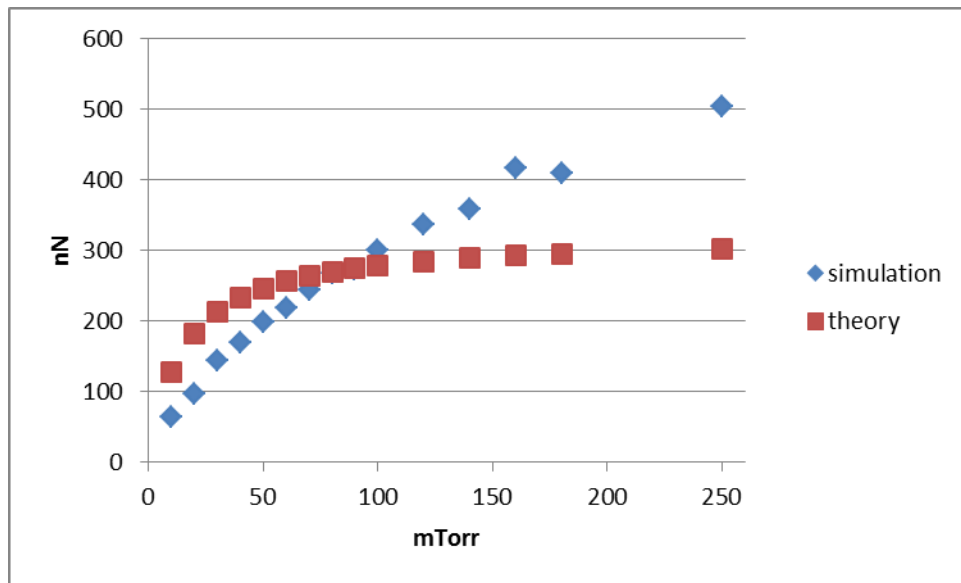


Fig. 19. Wide Vane Drag Force (simulation and theory). The vanes are 16mm by 16mm and have a 4mm stem connecting them to the spindle axis. They are rotating at 10 rad/s. The accommodation coefficient is 0.6.

The experimental results, simulation predictions, and theory predictions of the angular speed of both radiometers have a peak as a function of pressure between 20

mTorr and 90 mTorr. Quantitatively the differences at most pressures are less than an order of magnitude. The decrease in the angular speed at relatively higher pressures is more pronounced in the experiment than in the simulation or theory predictions. The difference between the asymptotic force values on the narrow vane and the wide vane in the thermal creep simulations causes the simulation prediction of the angular speed to be greater for the wide vane than the narrow vane. The theory prediction has the narrow vane faster than the wide vane at most pressures. The experimental results qualitatively match the theory predictions in this regard. Figures 20 and 21 compare the experimental results and simulation and theory predictions at the range of pressures examined.

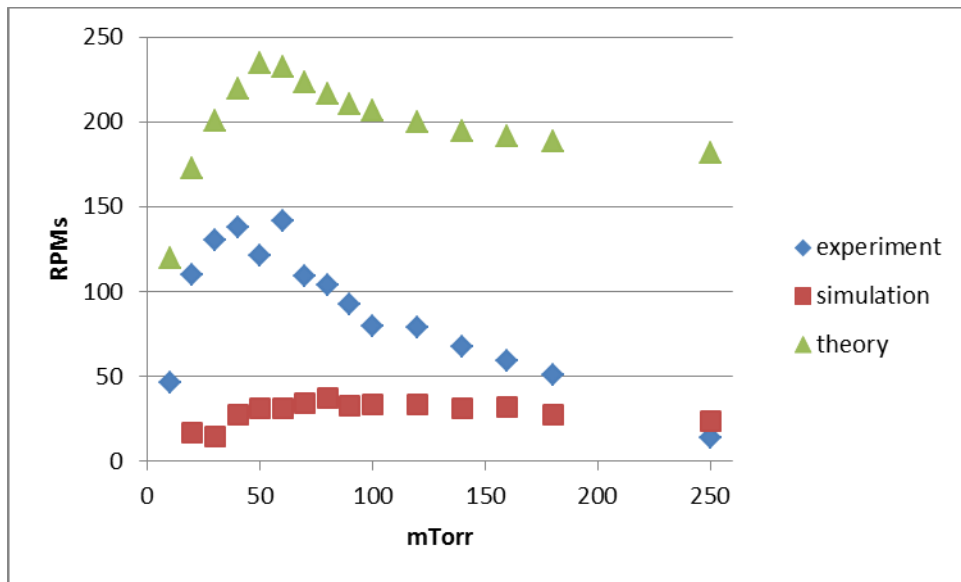


Fig. 20. Narrow Vane Angular Speed (experiment, simulation, and theory). The vanes are 8mm by 16mm. The temperature difference on the vanes is 9K. The characteristic length of the temperature gradient on the surfaces is 3.5mm. Positive angular speed represents rotation with the cold side leading.

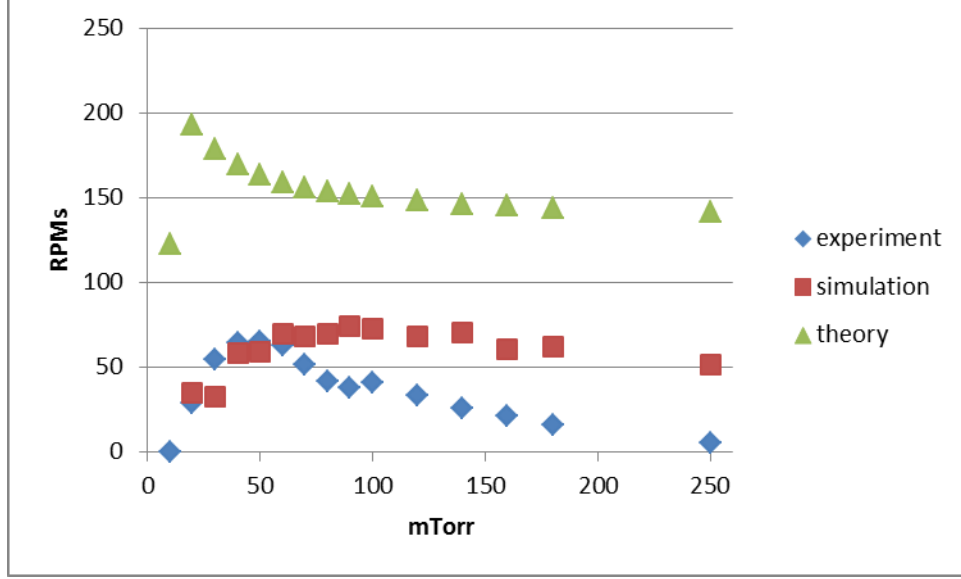


Fig 21. Wide Vane Angular Speed (experiment, simulation, and theory). The vanes are 16mm by 16mm. The radiometer has 4 vanes attached to the spindle by 4mm stems. The temperature difference on the vanes is 9K. The characteristic length of the temperature gradient on the vanes is 3.5mm. The temperature difference on the vanes is 9K. Positive angular speed represents rotation with the cold side leading.

VI. CONCLUSION

We have investigated the thermal creep shear force through experiment, kinetic theory calculations, and the DSMC simulations. All three investigations show the force acting from the hot to the cold side of the surface. The theory and the simulations both show the force rising with pressure and asymptotically approaching a constant value. The theory and the simulations both show the decrease in the radiometer's angular speed as a function of pressure at relatively higher pressures to be the result of increasing drag force rather than decreasing thermal creep force.

Left unexplained by our investigation is the difference in the asymptotic thermal creep force values on the narrow and the wide vanes in the DSMC results. Though this difference is not seen in the theory and is inconsistent with the experimental results, it is at least plausible the narrower vane is less effective at establishing a temperature gradient

in the gas either in reality or in a simulation with our particular setup. The results of future work with different experimental geometries and simulation setups or observing directly the gradient in the gas rather than just the force it creates on the surface will provide insight.

ACKNOWLEDGMENTS

The authors wish to thank Jeffery Catterlin, Steven Jacobs, Aaron Lopez, Jose Lopez, and Rebecca Marvin for running tests on various radiometers. D.W. wishes to thank Michael Gallis and Steve Plimpton for technical assistance with SPARTA and the Naval Postgraduate School Research Computing Group and Department of Defense High Performance Computing Modernization Program for the use of their equipment.

WORKS CITED

- [1] W. Crookes, "Researches on the Atomic Weight of Thallium," *Philosophical Transactions of the Royal Society of London*, vol. 163, pp. 277-330, 1873.
- [2] W. Crookes, "On Attraction and Repulsion Resulting from Radiation," *Philosophical Transactions of the Royal Society of London*, vol. 164, pp. 501-527, 1874.
- [3] O. Reynolds, "On the Forces Caused by Evaporation from, and Condensation at, a Surface," *Proceedings of the Royal Society of London*, vol. 22, pp. 401-401, 1874.
- [4] O. Reynolds, "On certain Dimensional Properties of Matter in the Gaseous State," *Philosophical Transactions of the Royal Society of London*, vol. 170, pp. 727-845, 1879.
- [5] J. C. Maxwell, "On Stresses in Rarified Gases Arising from Inequalities of Temperature," *Philosophical Transactions of the Royal Society of London*, vol. 170, pp. 231-256, 1879.
- [6] L. B. Loeb, *The Kinetic Theory of Gases*, New York: McGraw-Hill Book Company, 1934.
- [7] A. Ketsdever, N. Gimelshein, S. Gimelshein and N. Selden, "Radiometric phenomena: From the 19th to the 21st century," *Vacuum*, vol. 86, pp. 1644-1662, 2012.

- [8] M. Czerny and G. Hettner, "Messungen der thermischen Gleitung Gasen," *Zeitschrift fur Physik*, vol. 30, no. 1, pp. 258-267, 1924.
- [9] R. Marvin, Master's Thesis, Monterey: Naval Postgraduate School, 2012.
- [10] A. Lopez, J. Lopez, A. Larraza and D. Wolfe, "Maxwell and Crookes Radiometers," 2 December 2015. [Online]. Available: <https://www.youtube.com/watch?v=6jhNyA-SoSA>.
- [11] M. Scandurra, F. Iacopetti and P. Colona, "Gas Kinetic Forces on Thin Plates in the Presence of Thermal Gradients," *Physical Review E*, vol. 75, no. 2, pp. 0263081-0263085, 2007.
- [12] S. Chapman and T. G. Cowling, *The Mathematical Theory of Non-Uniform Gases*, Cambridge: University Press, 1952.
- [13] S. Song and M. M. Yovanovich, "Correlation of Thermal Accommodation Coefficient for 'Engineering' Surfaces," in *National Heat Transfer Conference*, Pittsburgh, 1987.
- [14] Y. H. Kuo, "On the Flow of an Incompressible Viscous Fluid Past a Flat Plate at Moderate Reynolds Numbers," *The Journal of Mathematics and Physics*, pp. 83-101, 1953.
- [15] A. M. Jones and J. G. Knudsen, "Drag Coefficients at Low Reynolds Numbers For Flow Past Immersed Bodies," *A.I.Ch.E. Journal*, vol. 7, no. 1, pp. 20-25, 1961.
- [16] Z. Janour, *Resistance of a Plate in Parallel Flow at Low Reynolds Numbers*, Washington: NACA TM 1316, 1951.
- [17] E. H. Kennard, *Kinetic Theory of Gases*, New York: McGraw-Hill Book Company, 1938.
- [18] G. Bird, *Molecular Gas Dynamics and the Direct Simulation of Gas Flows*, Oxford: Clarendon Press, 1994.
- [19] F. J. Alexander, A. L. Garcia and B. J. Alder, "Cell Size Dependence of Transport Coefficients in Stochastic Particle Algorithms," *Physics of Fluids*, vol. 10, no. 6, pp. 1540-1542, 1998.
- [20] A. L. Garcia and W. Wagner, "Time Step Truncation Error in Direct Simulation Monte Carlo," *Physics of Fluids*, vol. 12, no. 10, pp. 2621-2633, 2000.
- [21] M. A. Gallis, J. R. Torczynski, S. J. Plimpton, D. J. Rader and T. Koehler, "Direct Simulation Monte Carlo: The Quest for Speed," in *Proceedings of the 29th Rarefied Gas Dynamics Symposium*, Xi'an, 2014.
- [22] [Online]. Available: <http://sparta.sandia.gov>.
- [23] N. Selden, C. Ngalande, N. Gimelshein, S. Gimelsein and A. Ketsdever, "Origins of Radiometric Forces on a Circular Vane with a Temperature Gradient," *Journal of Fluid Mechanics*, vol. 634, pp. 419-431, 2009.
- [24] C. White, C. Colombo, T. J. Scanlon, C. R. McInnes and J. M. Reese, "Rarefied gas effects on the aerodynamics of high area-to-mass ratio spacecraft in orbit," *Advances in Space Research*, vol. 51, pp. 2112-2124, 2013.